

NUCLEAR STRUCTURE OF NEUTRON-DEFICIENT Au AND Pt ISOTOPES FROM HIGH-RESOLUTION LASER SPECTROSCOPY AT ISOLDE*

J. SAUVAGE^a, L. CABARET^b, J. CRAWFORD^c, H.T. DUONG^b, J. GENEVEY^d,
M. GIROD^e, A. GIZON^d, D. HOJMAN^{a†}, G. HUBER^f, F. IBRAHIM^d,
A. KNIPPER^g, M. KRIEG^f, F. LE BLANC^a, J.K.P. LEE^c, D. LUNNEY^{a‡},
G. MARGUIER^h, J. OBERT^a, J. OMS^a, J. PINARD^b, J.C. PUTAUX^a,
B. ROUSSIÈRE^a, V. SEBASTIAN^f, A. WOJTASIEWICZⁱ, S. ZEMLYANOV^{a§},
D. FORKEL-WIRTH^j, J. LETTRY^j
AND THE ISOLDE COLLABORATION

^a Institut de Physique Nucléaire, 91406 Orsay cedex, France

^b Laboratoire Aimé Cotton, 91405 Orsay cedex, France

^c Foster Radiation Laboratory, McGill University, H3A2T8 Montréal, Canada

^d Institut des Sciences Nucléaires, 38026 Grenoble cedex, France

^e Service de Physique Nucléaire, CEA, BP 12, 91680 Bruyères-le-Châtel, France

^f Institut für Physik der Universität Mainz, 55099 Mainz, Germany

^g Institut de Recherches Subatomiques, BP 28, 67037 Strasbourg cedex 2, France

^h Institut de Physique Nucléaire, 69622 Villeurbanne cedex, France

ⁱ Warsaw University, Warsaw, Poland

^j CERN, 1211 Geneva 23, Switzerland

(Received January 19, 1999)

Atomic spectroscopy measurements were carried out using the COMPLIS setup installed at the ISOLDE-BOOSTER facility. Hyperfine structure (HFS) spectra and isotope shift (IS) values were obtained for the neutron-deficient $^{178-185}\text{Pt}$ and for $^{184}\text{Au}^{g,m}$, providing deformation parameters β , magnetic moments μ and spectroscopic quadrupole moments (for $I \geq 1$) Q_s . In Pt isotopes, a deformation drop for $A = 178$ and an inverted odd-even staggering for the charge radius around the neutron mid-shell $N = 104$, have been observed very clearly. Furthermore, deformation changes $\delta\beta$ between isomeric and ground states for $^{183,185}\text{Pt}$ and ^{184}Au have been put forward. Thus, the influence of the proton-neutron coupling on the $\delta\beta$ value in ^{184}Au relatively to that in its isotone ^{183}Pt has been determined. Besides, the $h_{9/2}$ proton state that is decoupled from the core in $^{183,185}\text{Au}$, becomes the $3/2$ [532] state strongly coupled in ^{184}Au . The spin and parity values $I^\pi = 3^+$ have been assigned to the ^{182}Ir ground state from internal conversion electron measurements to prepare atomic spectroscopy studies in the Ir isotopic series.

PACS numbers: 21.10.-k, 21.10.Ft, 27.70.+q, 21.10.Ky

* Presented at the International Conference "Nuclear Physics Close to the Barrier", Warszawa, Poland, June 30–July 4, 1998.

† Permanent address: Departamento de Fisica, CNEA, 1429 Buenos Aires, Argentina

‡ Permanent address: CSNSM, 91405 Orsay cedex, France

§ Permanent address: Flerov Laboratory of Nuclear Reaction, JINR, Dubna 141980, Moscow Region, Russia

1. Introduction

The neutron-deficient Hg, Au and Pt nuclei are located in a region where nuclear shape instabilities exist. Indeed, shape coexistence phenomena and related shape transitions between two neighbouring isotopes have already been discovered in some of these nuclei. In Hg isotopes, a shape coexistence has been observed in ^{185}Hg : the $1/2^-$ ground state corresponds to a prolate shape while the $13/2^+$ isomeric state has an oblate or triaxial shape [1-3]. Thus, the huge odd-even staggering of the nuclear charge radius present from ^{186}Hg down to ^{181}Hg could be interpreted as alternating shape transitions: the even nuclei having an oblate or triaxial shape and the odd ones a prolate shape [4]. In Au nuclei, an oblate or triaxial to a prolate shape transition was put forward between ^{187}Au and ^{186}Au [2, 5-9]. These shape coexistence and transitions are illustrated in figure 1 by the observed mean square charge radius variations that indicate abrupt deformation changes. As for Pt isotopes, the moment of inertia of the rotational band built on the ground states of the even Pt nuclei increases between $A = 198$ and $A = 184$, remains almost constant between $A = 184$ and $A = 178$ and decreases below $A = 178$ [10] (see Fig. 2). Besides, the deformation change measured between ^{186}Pt and ^{185}Pt ground states could be understood as an oblate or triaxial to prolate shape transition [11]. On the other hand, the $1/2^-$ isomeric state of ^{185}Pt has a deformation similar to that of ^{186}Pt [12] though all the ^{185}Pt states lying at low energy could be explained with only a prolate shape [13]. Therefore, the goal of the experiment we performed on Pt atoms was to investigate the shape evolution and nuclear structure of the isomeric and ground states of the neutron-deficient isotopes farther from stability when the neutron number passes below the neutron mid-shell $N = 104$. Furthermore, experiments on the odd- A Pt and doubly-odd ^{184}Au isotopes aimed to precisely determine the influence of the neutron and proton coupling on nuclear deformation.

It is well known that atomic spectroscopy is a powerful method to investigate the properties of nuclei in their isomeric and ground states. Changes of the nuclear mean square charge radius $\delta\langle r_c^2 \rangle$ are extracted from isotope shift (IS) measurements, which provide information on nuclear deformation evolution along isotopic series. For odd and doubly-odd nuclei, magnetic moments, μ_I , can be deduced from hyperfine structure (HFS) spectra, which signs the nuclear structure of states. Moreover, spectroscopic quadrupole moments, Q_s , of nuclear states with spin values higher than $1/2$ are also deduced from HFS measurements, which gives the deformation sign for axially symmetric nuclei. Since, at the present time, Au and Pt beams are not delivered by isotope separators, such a laser spectroscopy method has to be performed on secondary beams. So, we used the COMPLIS setup which has

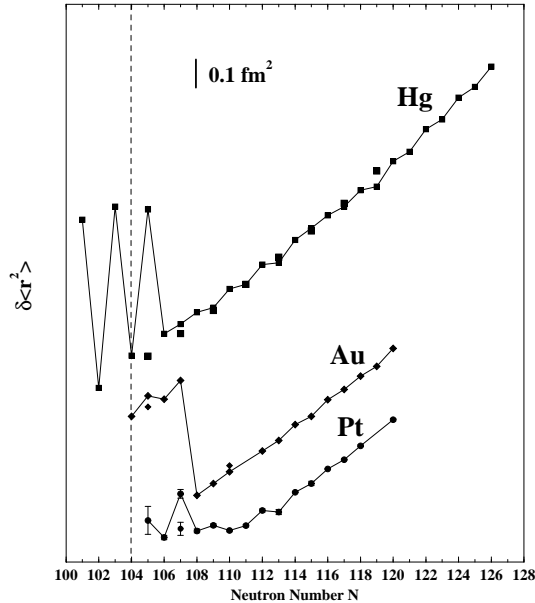


Fig. 1. $\delta\langle r_c^2 \rangle$ values extracted from IS results for Hg, Au and Pt nuclei [4,7-9,11,12].

been designed to realize Resonance Ionization Spectroscopy (RIS) study on a pulsed secondary atomic beam produced by laser desorption. IS and HFS spectra have been obtained for the $^{178-185}\text{Pt}$ atoms and $^{184}\text{Au}^{m,g}$ isomers. In a first part, after a brief description of the experimental setup, the results obtained on Pt and ^{184}Au isotopes will be presented, compared with theoretical predictions and discussed. After that, the deformation determined for the two isotones $^{183}\text{Pt}^{m,g}$ and $^{184}\text{Au}^{m,g}$ together with theoretical predictions will be used to qualitatively explain the relative location in energy of the isomeric and ground states of ^{184}Au that is inverted in comparison with that observed, for the same neutron states, in the other $N = 105$ isotones ^{181}Os , ^{182}Ir , ^{183}Pt and ^{185}Hg [2, 3, 13-20]. It is worth noting that the numerous nuclear spectroscopy measurements previously performed on Pt and Au isotopes were extremely helpful to prepare the present experiments and to interpret the results obtained. In a second part, to illustrate that atomic and nuclear spectroscopy are complementary methods, the case of the ^{182}Ir isotope [17, 18] in which it was necessary to establish if an isomeric state exists or not before measuring its HFS spectrum, will be used, as an example. The internal conversion electron measurement performed for that purpose will be described and the results presented. Lastly, some concluding remarks will be given.

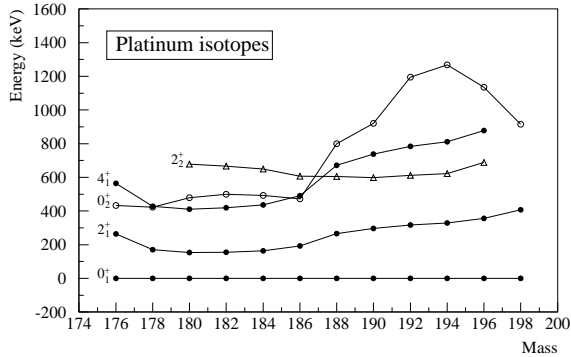


Fig. 2. Ground state bands, 0_2^+ and 2_2^+ levels through the even Pt nuclei.

2. Laser spectroscopy studies

2.1. Experimental setup and procedure for measurements on Pt atoms

At the present time, Pt atoms are only obtained by two successive β^+ /EC decays or α decay of Hg ions. At ISOLDE, Hg isotopes are produced by bombarding the molten lead target with the 1 GeV staggered proton beam delivered by the PS-BOOSTER [21]. They are extracted from the ion source using a 60 kV high voltage and mass-separated by the General Purpose Separator. The 60 kV Hg beam from ISOLDE is guided by electrostatic elements and a magnet and then slowed from 60 kV down to 1 kV in a retardation lens before being deposited onto a graphite collecting disk. After a waiting time defined in order to optimize the amount of the daughter or grand-daughter of Hg atoms, Pt atoms are desorbed by a powerful frequency-doubled Nd:YAG laser beam producing the pulsed secondary Pt atomic beam. Some μ s later the desorbed atoms are ionized in a three step RIS process. The resulting ions are then extracted under the 59 kV high voltage and guided to the microchannel plate detector. They are mass-identified by their time-of-flight. For each frequency step, the ion signal is integrated using a digital oscilloscope and the data are sent in a multi-task SUN workstation. An injector serves to send stable ion beam into the COMPLIS incident beam line before the experiment in order to optimize the experimental conditions. Spectroscopic information is provided by the frequency scan of the first laser excitation step at 306 nm wavelength that corresponds to the $5d^9 6s^3 D_3 \rightarrow 5d^9 6p^3 P_2$ atomic transition.

To produce single mode pulses a dye cell pumped by frequency-doubled Nd:YAG pulses is inserted in the cavity of a continuously tunable single mode dye laser [22]. These pulses are then amplified in dye cells and frequency-doubled in a crystal to get the single mode beam at 306 nm wavelength. A

commercial dye laser pumped by a Nd:YAG delivers a pulsed laser beam at around 741 nm for the ionizing step ; its frequency-doubled beam at 371 nm is used to induce the second excitation step. The COMPLIS setup has also been used for ^{184}Au measurements [23].

2.2. Experimental results

The HFS spectra of the $^{183}\text{Pt}^g$ and $^{185}\text{Pt}^{m,g}$ atoms were more precisely measured. Furthermore, the HFS spectra of $^{178,179,180,181,182}\text{Pt}$ and $^{183}\text{Pt}^m$ atoms were recorded for the first time. The HFS spectrum of ^{183}Pt obtained from the 306 nm atomic transition is shown in figure 3, as an example. The vertical scale has been chosen to emphasize the weak peaks corresponding to the $7/2^-$ isomer ($T_{1/2}=43$ s) ; the two strongest peaks that are saturated, correspond to the $1/2^-$ ground state ($T_{1/2}=6.5$ m). Since the half-lives of the two isomers are very different the peaks could be easily identified by use of different waiting times, 57 s and 172 s, between the end of the Hg ion collection and the laser desorption.

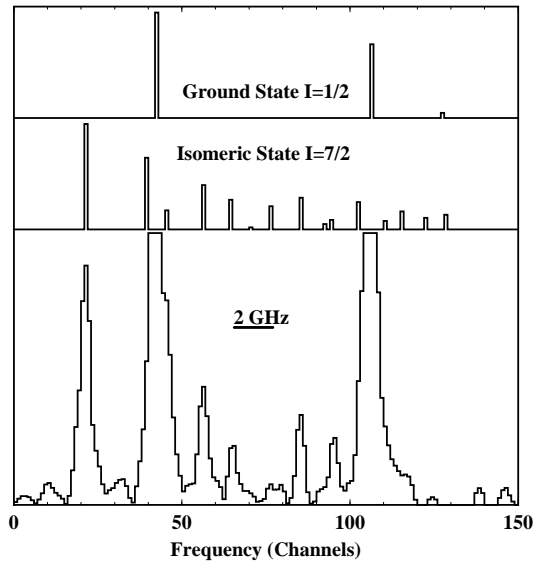


Fig. 3. Hyperfine spectrum of ^{183}Pt .

For the odd isotopes with a nuclear spin value $I = 1/2$ only the magnetic moment can be determined. It is given by the following relation: $\mu = AIJ/H_e(0)$. The magnetic field at the nucleus $H_e(0)$ is calculated from the well known μ and A values of ^{195}Pt [24, 25]. The magnetic hyperfine constants for the two atomic levels A and A' are determined from the frequency positions of the resonant lines. For $^{183}\text{Pt}^m$ and $^{185}\text{Pt}^g$, in addi-

tion to the magnetic moment, it is possible to determine the spectroscopic quadrupole moment Q_s : $Q_s = B/e\phi_{JJ}(0)$. The electric field gradient at the nucleus is known [12] ; thus $Q_s = -0.685B$. The electrostatic hyperfine constants B and B' are also extracted from the frequency positions of the resonant lines. The nuclear moments obtained are given in Table I. Q_s^{corr} is

TABLE I

Nuclear moments of platinum isotopes.

A	I^π, K	μ (μ_N)	Q_s (b)	Q_s^{corr} (b)	Q_0 (b)	β
185 ^g	9/2 ⁺ , 9/2	-0.723(11)	+4.10(19)	+3.73(17)	+6.84(31)	+0.229(10)
185 ^m	1/2 ⁻ , 1/2	+0.503(5)				
183 ^g	1/2 ⁻ , 1/2	+0.502(5)				
183 ^m	7/2 ⁻ , 7/2	+0.782(14)	+3.71(13)	+3.37(27)	+7.22(58)	+0.242(18)
181	1/2 ⁻ , 1/2	+0.484(21)				
179	1/2 ⁻ , 1/2	+0.431(32)				

the spectroscopic quadrupole moment corrected for core polarization effects:

$$Q_s^{\text{corr}} = Q_s / (1 - R).$$

The Sterheimer shielding factor $R = -0.1$ is obtained from systematics on the $5d$ shell [26]. Q_0 is the intrinsic quadrupole moment obtained if we assume an axial symmetry for the nucleus:

$$Q_0 = Q_S^{\text{corr}}(I + 1)(2I + 3) / (3K^2 - I(I + 1)),$$

where K is the projection, on the symmetry axis, of the angular momentum I . The deformation parameter is deduced from the value by use of the following relation with $r_0 = 1.2$ fm:

$$Q_0 = \frac{3}{\sqrt{5}\pi} Z r_0^2 A^{\frac{2}{3}} \beta (1 + \frac{2}{7} \sqrt{\frac{5}{\pi}} \beta).$$

The IS values relative to ^{194}Pt are extracted from the experimental spectra of all isotopes. It consists of a mass shift and a field shift $\delta\nu$. The mass shift contribution that varies as $1/A^2$ is very small for the masses around $A = 180$ [12]. The nuclear parameter $\lambda^{A,A'}$ is extracted from the field shift: $\lambda^{A,A'} = \delta\nu^{A,A'} / F_{306}$, where the electronic factor F_{306} of the 306 nm atomic transition has been estimated from a King plot made on the stable isotopes using the calculated F_{266} value of the 266 nm transition [12] and the experimental IS data of both the 306 nm and 266 nm transitions: $F_{306} = -18.5$

GHz/fm². From the $\lambda^{A,A'}$ values we deduce: the $\delta\langle r_c^2 \rangle$ values; and then, assuming a pure quadrupole deformation, the $\langle \beta^2 \rangle^{1/2}$ values with the β value of ¹⁹⁴Pt (obtained from B(E2) measurements) used as a reference. The IS

TABLE II
Mean square charge radius changes in platinum isotopes.

<i>A</i>	<i>I</i> ^π	$\delta\nu^{194,A}$ (GHz)	$\delta\langle r_c^2 \rangle$ (fm ²)	$\langle \beta^2 \rangle^{1/2}$	β ¹
185 ^g	9/2 ⁺	1.582(35)	-0.093(7)	0.231(3)	+0.229(10)
185 ^m	1/2 ⁻	3.611(7)	-0.212(6)	0.207(3)	
183 ^g	1/2 ⁻	3.67 (5)	-0.216(8)	0.227(3)	
183 ^m	7/2 ⁻	1.81 (4)	-0.106(8)	0.246(3)	+0.242(18)
182	0	4.75 (8)	-0.279(10)	0.225(4)	
181	1/2 ⁻	4.27 (20)	-0.251(15)	0.239(4)	
180	0	6.13 (5)	-0.360(11)	0.229(4)	
179	1/2 ⁻	5.70 (30)	-0.335(21)	0.243(5)	
178	0	8.99 (20)	-0.529(16)	0.216(5)	

¹deformation parameters deduced from *Q*₀ values

results are given in Table II where the β values deduced from the *Q*₀ values have been reported in the last column. The nuclear moments, IS results and deformation parameters of ¹⁸⁴Au, taken from reference 23, are reported in Table III. For ¹⁸⁵Pt^g, ¹⁸³Pt^m and ¹⁸⁴Au^g, the β value deduced from the *Q*₀ value is in excellent agreement with the value calculated from the IS result, which shows that the axial symmetry we assumed to calculate *Q*₀ is fully justified.

TABLE III
Nuclear moments and IS results in ¹⁸⁴Au from reference [23].

<i>A</i>	<i>I</i> ^π , <i>K</i>	<i>Q</i> _s (b)	<i>Q</i> ₀ (b)	$\delta\nu^{197,A}$ (GHz)	$\delta\langle r_c^2 \rangle$ (fm ²)	β ₁	$\langle \beta^2 \rangle^{1/2}$ ₂
184 ^g	5 ⁺ , 5	+4.65(26)	+8.06(45)	2.81(30)	-0.064(12)	+0.264(14)	0.255(3)
184 ^m	2 ⁺ , 2	+1.90(16)	+6.65(56)	4.20(30)	-0.100(12)	+0.221(17)	0.249(3)

¹ β deformation parameters deduced from *Q*₀ values
² $\langle \beta^2 \rangle^{1/2}$ deformation parameters from IS results

The $\delta\langle r_c^2 \rangle$ measured in the Pt isotopes are shown in figure 4. The most remarkable results are the following: a) a large deformation change between the isomeric and ground states for both ¹⁸³Pt and ¹⁸⁵Pt, b) a strong inverted odd-even staggering around the neutron mid-shell *N* = 104, c) for the even

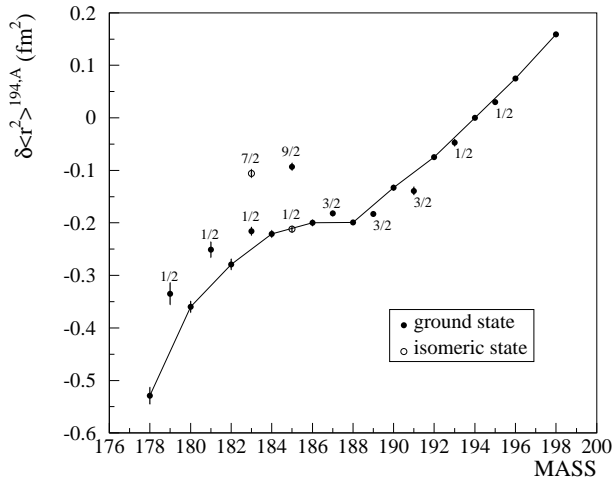


Fig. 4. $\delta\langle r_c^2 \rangle$ values for Pt isotopes from the present work and references [11,12].

Pt, a clear deformation increase from $A = 188$ down to $A = 180$ and a decrease for $A = 178$. Therefore, the maximum of the deformation is found for $N = 102$. This deformation evolution is in agreement with the moment of inertia change observed in the ground state rotational bands shown in figure 2.

2.3. Brief description of the theoretical approaches

To attempt to interpret all of these results, two different theoretical approaches have been used: the first one to predict the energies and the magnetic moments of the states in the odd nuclei; the second one to study the $\delta\langle r_c^2 \rangle$ values:

— State energies and magnetic moments

In this approach we proceed in three steps. First, assuming axial symmetry, Hartree-Fock + BCS calculations are performed using the Skyrme III force to get the quasiparticle wave functions ψ for the core [27]. Furthermore, the core has been constrained to take the deformation extracted from our $\delta\langle r_c^2 \rangle$ measurement for the odd nucleus. Second, using these wave functions in an axial rotor + quasiparticle coupling model the wave functions Ψ for the coupled states of the odd nucleus are obtained. In this coupling model the Coriolis interaction is exactly treated and all the quasiparticle states ψ located at ± 5 MeV around the Fermi level are taken into account [28]. Lastly the magnetic moments are calculated using the wave functions Ψ and $g_R = Z/A$ [29].

— $\delta\langle r_c^2 \rangle$ values

Microscopic Hartree–Fock–Bogoliubov (HFB) calculations using the Gogny force have been carried out in two ways [30, 31]. First, calculations are made, assuming axial symmetry, to get the potential energy curve. The static charge radius is determined for the energy minimum of the curve. The blocking procedure is adopted for the odd nuclei [31]. Second, for the even nuclei, HFB calculations are performed to get the potential energy surface against the deformation parameters β and γ , collective masses and moments of inertia. And then, using these ingredients a collective Hamiltonian treating quadrupole motion is built microscopically and solved. The obtained wave functions serve to calculate the dynamic mean square charge radius.

It is worth noting that in these two microscopic approaches there is no adjustable parameters.

2.4. Discussion

The experimental $\delta\langle r_c^2 \rangle$ values are compared with those calculated using the axial HFB approach in figure 5a. Contrary to the experimental results the odd-even staggering is predicted to be normal. Such a normal odd-even staggering that corresponds to larger $\langle r_c^2 \rangle$ values for even–even nuclei than for odd nuclei is usually explained by pairing effects [32]. Besides, a too sharp radius change is calculated between ^{188}Pt and ^{186}Pt , and the nuclei are predicted too much deformed especially for the lightest even–even isotopes. On the other hand, the radius change between the isomeric and ground states are correctly reproduced for both ^{183}Pt and ^{185}Pt . For the even–even Pt, the experimental results are compared with the theoretical ones obtained using the triaxial HFB calculations (see Fig. 5b). Though the predicted deformations remain slightly too large for the lightest isotopes, the agreement between the experimental and theoretical $\delta\langle r_c^2 \rangle$ values is very clearly improved. The deformation change is quite well reproduced but it is slightly more drastic. A plateau is observed from ^{188}Pt down to ^{184}Pt whereas the model predicts a slope change between ^{188}Pt and ^{184}Pt . However, the slope change is found for the same mass $A = 188$ and the experimental and theoretical curves have very similar trends. Furthermore, one can see by comparing the figures 5a and 5b that the inverted odd-even staggering can be qualitatively explained if the even–even Pt nuclei have a triaxial shape with γ values $\sim 15^\circ$ and the odd Pt a pure prolate shape. A very remarkable feature that remains to be understood, is the regular increase of the odd-even staggering when the neutron number decreases (see Fig. 4).

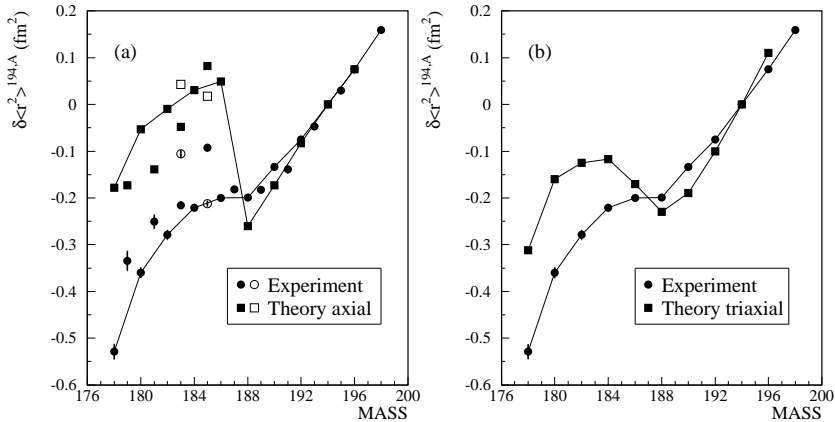


Fig. 5. (a) — Comparison of the measured $\delta\langle r_c^2 \rangle$ values with the static $\delta\langle r_c^2 \rangle$ values from the axial HBF approach. (b) — Comparison of the experimental $\delta\langle r_c^2 \rangle$ values with the dynamic $\delta\langle r_c^2 \rangle$ values from the triaxial HBF approach.

TABLE IV

Comparison of the measured μ_{exp} and calculated μ_{cal} magnetic moments.

Nucleus	I^π	Configuration	μ_{exp} (μ_N)	μ_{cal} $g_{s\text{free}}(0.6g_{s\text{free}})$
$^{185}\text{Pt}^g$	$9/2^+$	$9/2^+[624]$	$-0.723(11)$	$-1.46(-0.86)$
$^{185}\text{Pt}^m$	$1/2^-$	$1/2^- [521]$	$+0.503(5)$	$+0.63(+0.37)$
$^{183}\text{Pt}^g$	$1/2^-$	$1/2^- [521]$	$+0.502(5)$	$+0.63(+0.37)$
$^{183}\text{Pt}^m$	$7/2^-$	$7/2^- [514]$	$+0.782(14)$	$+1.46(+0.99)$
^{181}Pt	$1/2^-$	$1/2^- [521]$	$+0.484(21)$	$+0.63(+0.38)$
^{179}Pt	$1/2^-$	$1/2^- [521]$	$+0.431(32)$	$+0.64(+0.38)$
$^{184}\text{Au}^g$	5^+	$\pi 3/2^- [532] \otimes \nu 7/2^- [514]$	$+2.07(2)$	$+2.3(2.2)$
$^{184}\text{Au}^m$	2^+	$\pi 3/2^- [532] \otimes \nu 1/2^- [521]$	$+1.44(2)$	$+1.2(1.4)$

The measured magnetic moments μ_{exp} of Pt nuclei are compared in Table IV with the magnetic moments μ_{cal} calculated using the axial-rotor+one-quasiparticle coupling model for $g_s = g_{s\text{free}}(0.6g_{s\text{free}})$. A satisfactory agreement is obtained, which confirms the structure, corresponding to a prolate shape, attributed to the isomeric and ground states of the odd Pt nuclei. In ^{184}Au , our measurements have shown that the 5^+ and 2^+ states have almost pure $K = 5$ and $K = 2$ wave functions. Then, they correspond very likely to the $\pi 3/2[532] \otimes \nu 7/2[514]$ and $\pi 3/2[532] \otimes \nu 1/2[521]$ configurations respectively. It is worth noting that the $h_{9/2}$ proton, decoupled from the core by the Coriolis force in $^{183,185}\text{Au}$ [2, 6], becomes the strongly

coupled $3/2[532]$ proton state ($h_{9/2}$ parentage) in the doubly-odd ^{184}Au nucleus. The magnetic moments could be then estimated using the relation $\mu = K(g_{Kp}K_p + g_{Kn}K_n + g_R)/(I + 1)$ [33] and the g_{Kp} and g_{Kn} values deduced from magnetic moments calculated in the neighbouring odd isotopes. The perfect agreement obtained between μ_{exp} and μ_{cal} strongly confirms the configurations attributed to both states (see Table IV).

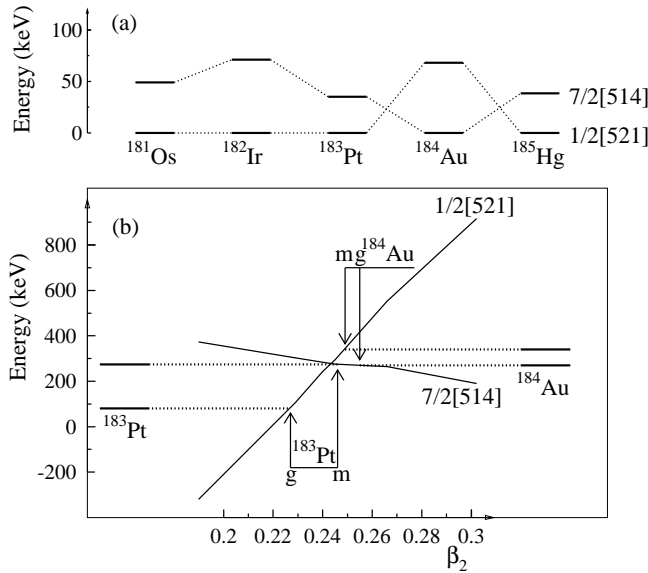


Fig. 6. (a) — Systematics of the $1/2[521]$ and $7/2[514]$ neutron states (coupled, in the case of the doubly-odd nuclei, to the proton state arising from the $h_{9/2}$ subshell) for the $N = 105$ isotones. (b) — Theoretical energies of the $1/2[521]$ and $7/2[514]$ neutron states against β .

The systematics of the $1/2[521]$ and $7/2[514]$ neutron states (coupled to the proton coming from the $h_{9/2}$ subshell in the case of the doubly-odd nuclei) observed in the $N = 105$ isotones, is shown in figure 6a. There is an inversion of the $1/2$ and $7/2$ states in ^{184}Au relatively to other $N = 105$ isotones. In order to know if this state inversion is due or not to the deformation changes observed in $^{183}\text{Pt}_{g,m}$ and $^{184}\text{Au}_{g,m}$ we have calculated the evolution of the energy of the $1/2[521]$ and $7/2[514]$ neutron states as a function of the deformation using the axial-rotor+one-quasiparticle coupling model with the neighbouring ^{184}Pt core. The results are shown in figure 6b together with the deformations deduced from our measurements for the isomeric and ground states of ^{183}Pt and ^{184}Au . One can see that the $1/2[521]$ state lies below the $7/2[514]$ state for the ^{183}Pt deformations whereas it lies above for the ^{184}Au ones. Thus the deformations measured for $^{183}\text{Pt}_{g,m}$ and

$^{184}\text{Au}^{g,m}$ allow us to qualitatively explain the state inversion observed in ^{184}Au . Moreover, the difference in deformation between the isomeric and ground states of ^{184}Au is clearly smaller than that in ^{183}Pt . This is due to the coupling of the $1/2[521]$ and $7/2[514]$ neutron states to the $3/2[532]$ proton state that tends to increase the nuclear deformation.

3. Internal conversion electron measurements

The Ir isotopic series is a very good candidate for studying the $h_{9/2}$ proton coupling mode since the proton state arising from the $h_{9/2}$ subshell plays an important role in most of the isomeric and ground states of the neutron-deficient Ir isotopes. To illustrate the fact that atomic and nuclear spectroscopy are complementary methods I will use the case of ^{182}Ir , isotone of ^{184}Au . An in-beam study previously performed in ^{182}Ir allowed Kreiner *et al.* [18] to identify three rotational bands. A doubly-decoupled band built on the level located at the lowest energy has been associated to the $\pi h_{9/2} \otimes \nu 1/2[521]$ configuration. Spin and parity values $I^\pi = 5^+$ have been assigned to its observed bandhead from the known properties of doubly-decoupled bands [34,35]. The 3^+ state of this band is expected to be located below and very close to the 5^+ state [36]. The second observed rotational band possibly corresponds to the $\pi h_{9/2} \otimes 7/2[514]$ configuration. It decays to the first band via a 45.4 keV M1 transition. The third band of a semi-decoupled type has been associated to the $\pi h_{9/2} \otimes \nu i_{13/2}$ configuration. It decays to the second band by a 81.5 keV E1 transition. Furthermore, the low-spin states of ^{182}Ir have been studied using the β^+/EC decay of ^{182}Pt [17]. The two important lines linking the rotational bands mentioned above

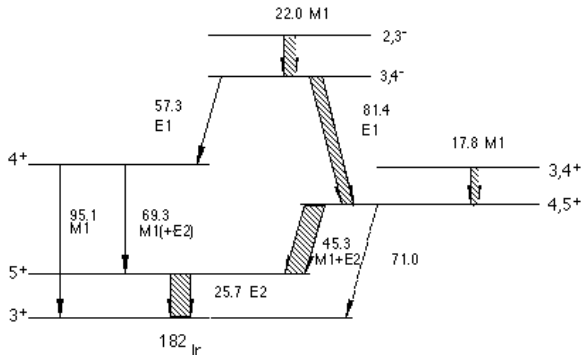


Fig. 7. The lowest energy part of the ^{182}Ir level scheme established from β^+/EC decay of ^{182}Pt [17]. The E2 25.7 keV transition has been added.

have also been observed (see Fig. 7). They form a cascade 81.4–45.3 keV that feeds a state located at 25 keV above the ground state. Given that 20% of the total desintegration intensity populates this 25 keV level it was concluded that either the 25 keV level is an isomeric state or the decaying transition is highly converted and has, at least, an E2 multipolarity. An E2 25 keV transition, if it exists can be observed only through its internal conversion electrons. So to search for, a radioactive decay experiment was performed at ISOLDE using the molten lead target [21] to produce a Hg mass-separated beam.

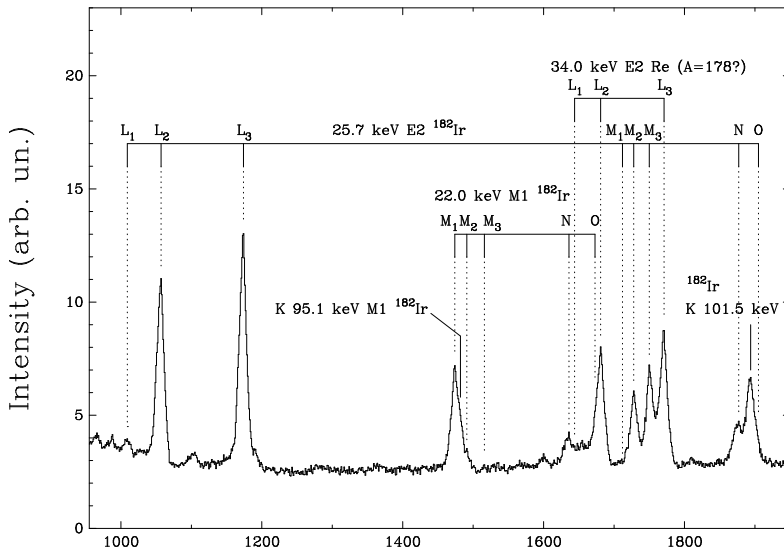


Fig. 8. Low-energy part of the electron spectrum from the β^+ /EC decay of ^{182}Pt .

The ^{182}Pt nuclei were produced by two successive β^+ /EC decays of ^{182}Hg nuclei. To perform the electron measurement a magnetic spectrograph was coupled to a tape transport system [37]. The radioactive ions are slowed from 60 kV down to 0.7 kV before collection to prevent an implantation into the tape. This preserves the high resolution for low-energy electrons. Moreover, -13 kV are applied to the source inside the spectrograph to accelerate the emitted electrons so that the low-energy electrons can be detected by the photographic film. The low-energy part of the electron spectrum recorded in this experiment is shown in figure 8. The electron lines for the internal conversion of a 25.7 keV transition in the L_1 , L_2 , L_3 , M_2 , M_3 and N subshells are very clearly observed. Their relative intensities are in perfect agreement with those expected for an E2 multipolarity, which unambiguously determines spin and parity¹ values $I^\pi = 3^+$ for the ^{182}Ir grounds state.

This 3^+ state is very likely the band head of the rotational band associated to the $\pi h_{9/2} \otimes \nu 1/2[521]$ configuration. No isomeric state with long half-life exists in ^{182}Ir . Laser spectroscopy experiment will allow the measurement of the nuclear moments, which should confirm the configuration proposed for the ground state and determine if the wave function is pure $K = 3$ or not, providing information on the coupling mode of the proton and neutron states.

4. Concluding remarks

From the laser spectroscopy results and their comparison with the axial and triaxial HFB calculations we can conclude that the inverted odd-even staggering observed in the light Pt isotopes is the signature of alternating shape transitions, the odd Pt nuclei having a prolate shape and the even-even Pt triaxial shape with γ values around 15° . The deformation parameter values extracted from IS measurements for ^{183}Pt and ^{184}Au allows us to qualitatively explain the state inversion observed in ^{184}Au relatively to its $N = 105$ isotones. Furthermore, they allow the determination of the increase of the deformation in $^{184}\text{Au}^g$ and $^{184}\text{Au}^m$ relatively to $^{183}\text{Pt}^m$ and $^{183}\text{Pt}^g$ due to the intruder $3/2[532]$ proton state coupling in ^{184}Au . For the even-even Pt isotopes, the deformation maximum is found for the neutron number $N = 102$ that is slightly beyond the neutron mid-shell $N = 104$. Atomic and nuclear spectroscopy are complementary methods to study nuclear structure. This becomes especially visible for the doubly-odd nucleus studies as shown for ^{184}Au and ^{182}Ir . Thus, an important result is the change of the proton coupling observed between the odd and doubly-odd nuclei. The $h_{9/2}$ proton that is decoupled from the core in $^{183,185}\text{Au}$, is strongly coupled in the doubly-odd ^{184}Au nucleus. Nuclear spectroscopy results strongly suggest that the $h_{9/2}$ proton is implied in the ground state of the Ir isotopes with $A < 187$. Therefore, the Ir isotopes are very good candidates to provide more information about the $h_{9/2}$ proton coupling modes.

REFERENCES

- [1] P. Dabkiewicz *et al.*, *Phys. Lett.* **82B**, 199 (1979).
- [2] C. Bourgeois *et al.*, *Nucl. Phys.* **A386**, 308 (1982) and references therein.
- [3] F. Hannachi *et al.* *Z. Phys.* **A330**, 15 (1988).
- [4] G. Ulm *et al.*, *Z. Phys.* **A325**, 247 (1986) and references therein.
- [5] M. G. Porquet *et al.*, *Nucl. Phys.* **A411**, 65 (1983).
- [6] M. I. Macias-Marques *et al.*, *Nucl. Phys.* **A427**, 205 (1984).

- [7] K. Wallmeroth *et al.*, *Nucl. Phys.* **A493**, 224 (1989).
- [8] G. Savard *et al.*, *Nucl. Phys.* **A512**, 241 (1990).
- [9] G. Passler *et al.*, *Nucl. Phys.* **A580**, 173 (1994).
- [10] G. D. Dracoulis *et al.*, *J. Phys. G* **12**, L97 (1986).
- [11] H.T. Duong *et al.*, *Phys. Lett.* **B217**, 401 (1989).
- [12] T. Hilberath *et al.*, *Z. Phys.* **A342**, 1 (1992).
- [13] B. Roussi re *et al.*, *Nucl. Phys.* **A504**, 511 (1989), *Nucl. Phys.* **A438**, 93 (1985).
- [14] Visvanathan *et al.*, *Phys. Rev.* **C19**, 282 (1979).
- [15] J. Nyberg *et al.*, *Nucl. Phys.* **A511**, 92 (1990).
- [16] B. Roussi re *et al.*, *Z. Phys.* **A351**, 127 (1995).
- [17] J. Sauvage *et al.*, *Nucl. Phys.* **A592**, 221 (1995).
- [18] A.J. Kreiner *et al.*, *Phys. Rev.* **C42**, 878 (1990).
- [19] F. Ibrahim *et al.*, *Z. Phys.* **A350**, 9 (1994).
- [20] F. Ibrahim *et al.*, *Phys. Rev.* **C53**, 1547 (1996).
- [21] J. Lettry *et al.*, *Nucl. Instrum. Methods* **B126**, 170 (1997).
- [22] J. Pinard, S. Liberman, *Opt. Commun.* **20**, 344 (1977).
- [23] F. Le Blanc *et al.*, *Phys. Rev. Lett.* **79**, 2213 (1997).
- [24] S. B ttgenbach *et al.*, *Z. Phys.* **A317**, 237 (1984).
- [25] P. Raghavan *et al.*, *At. Data Nucl. Data Tables* **42**, 189 (1989).
- [26] W. Childs, K. Cheng, *Phys. Rev.* **A30**, 667 (1984).
- [27] H. Flocard *et al.*, *Nucl. Phys.* **A203**, 433 (1973).
- [28] M. Meyer *et al.*, *Nucl. Phys.* **A316**, 93 (1979).
- [29] J. Libert *et al.*, *Phys. Rev.* **C25**, 586 (1982).
- [30] J. Decharg , D. Gogny, *Phys. Rev.* **C21**, 1568 (1980).
- [31] M. Girod *et al.*, *Phys. Rev.* **C37**, 2600 (1988).
- [32] D. Zawischa, *Phys. Lett.* **B155**, 309 (1985).
- [33] C. Ekstr m *et al.*, *Phys. Scr.* **14**, 199 (1976).
- [34] J. Davidson *et al.*, *Z. Phys.* **A324**, 363 (1986).
- [35] A. Ben Braham *et al.*, *Nucl. Phys.* **A533**, 113 (1991).
- [36] A. Ben Braham *et al.*, *Nucl. Phys.* **A482**, 553 (1988).
- [37] P. Kilcher *et al.*, *Nucl. Instrum. Methods* **A274**, 485 (1989).